Chapter 2
Laser Cooling

In this introductory chapter, we first consider the interaction of a two-level atom with a monochromatic laser field, by reviewing the emission and absorption radiation processes, as described by the semi-classical optical Bloch equations. We then discuss the basic principles of laser cooling, using both the momentum and the energy pictures. A simple expression for the laser cooling force is derived and the concept of Doppler temperature limit, characterizing the laser cooling process, is introduced. This is followed by a discussion of magnetic traps, with particular emphasis on the Helmholtz and Ioffe configurations, and a description of the magneto-optical trap.

With these basic ingredients in mind, we can then discuss the sub-Doppler cooling processes, which can lead the atomic gas to temperatures well below the Doppler temperature limit, and in particular, to Bose Einstein condensation. The first of these sub-Doppler processes is the celebrated Sisyphus cooling, which makes use of counter-propagating circularly polarized laser beams. The second is the evaporative cooling, which is known for long time to work at macroscopic level, but is also extremely efficient at cooling a confined atomic cloud, at the cost of a severe reduction of the number of confined atoms. The chapter finishes with a discussion of the sympathetic cooling, which can be used to cool down atomic and molecular gases for which the principles of laser cooling cannot directly be applied.

2.1 Atom in the Laser Field

In order to understand the main properties of the atom-laser interaction, we first consider the semi-classical approach, where we use a quantum description for a two-level atom but describe radiation as a classical field. The full quantum description of both atom and radiation is given in the Appendix. For a detailed account see, for instance [1–3]. This semi-classical description allows us to understand the emission

J.T. Mendonça and H. Terças, *Physics of Ultra-Cold Matter*, Springer Series on Atomic, Optical, and Plasma Physics 70, DOI 10.1007/978-1-4614-5413-7_2,

and absorption mechanisms of light by atoms. However, spontaneous emission can only be understood with the full quantum model, and its contribution is introduced phenomenologically here.

The semi-classical Hamiltonian operator relevant to this problem has two distinct parts

$$H = H_a + H_{\text{int}}, \tag{2.1}$$

where H_a is the unperturbed Hamiltonian of the atom, with the eigenvalue equation $H_a|j\rangle = E_j|j\rangle$. Here E_j are the energy values of the atomic quantum levels, with the corresponding eigenstates $|j\rangle$. We consider a simple two-level atom model, where $j = 1, 2$. In Eq. (2.1), we have also used the interaction Hamiltonian H_{int}, which describes the coupling between the atom and the laser field, as specified below. In the absence of the laser field, i.e. $H_{\text{int}} = 0$, the atomic state vectors have solutions of the form $|j, t\rangle = \exp(-iE_j t/\hbar)|j\rangle$. When $H_{\text{int}} \neq 0$, these atomic states become coupled by the radiation field, and the atomic state vector will contain a superposition of the two states, as described by

$$|\psi(\mathbf{r}, t)\rangle = \sum_{j=1,2} C_j(t) \exp(-iE_j t/\hbar)|j\rangle, \tag{2.2}$$

where the coefficients $C_j(t)$ satisfy the normalization condition $\langle\psi(\mathbf{r}, t)|\psi(\mathbf{r}, t)\rangle = |C_1(t)|^2 + |C_2(t)|^2 = 1$. The quantities $|C_j(t)|^2$ give the probability for the atom to be in the state j. In order to determine these probabilities, we consider the time dependent Schrödinger equation

$$i\hbar \frac{\partial}{\partial t}|\psi\rangle = (H_a + H_{\text{int}})|\psi\rangle. \tag{2.3}$$

Using the superposition of states (2.2), we can derive from here the following two evolution equations

$$i\hbar \frac{\partial C_1}{\partial t} = C_1 H_{11} + C_2 H_{12} e^{-i\omega_0 t}, \quad i\hbar \frac{\partial C_2}{\partial t} = C_1 H_{21} e^{i\omega_0 t} + C_2 H_{22} \tag{2.4}$$

where we have introduced the transition frequency $\omega_0 = (E_2 - E_1)/\hbar$, and used the matrix elements of the interaction Hamiltonian operator, $H_{ij} = \langle i|H_{\text{int}}|j\rangle$.

Before studying the solutions of Eq. (2.4), we need to discuss the explicit form of these matrix elements. Let us consider the generic case where the two quantum levels $|1\rangle$ and $|2\rangle$ are associated with the electron eigenstates in the atom. It is known that, in the Coulomb gauge, the interaction Hamiltonian is given by

$$H_{\text{int}} = \frac{e}{m}\mathbf{p} \cdot \mathbf{A}(\mathbf{r}, t) + \frac{e^2}{2m} A^2(\mathbf{r}, t). \tag{2.5}$$

where $\mathbf{A}(\mathbf{r}, t)$ is the vector potential associated with the radiation field. This expression can be simplified in the following way. First, for a low intensity radiation field, the quadratic term A^2 can be neglected. Second, we can usually

assume that the wavelength of the electromagnetic radiation is much larger than the dimensions of the atom. This is the so-called *dipole approximation*, which allows us to develop the vector potential $\mathbf{A}(\mathbf{r},t)$ around the atom position $\mathbf{r}_0 = 0$, as follows: $\mathbf{A}(\mathbf{r},t) = \mathbf{A}(t)\exp(i\mathbf{k}\cdot\mathbf{r}) \simeq \mathbf{A}(t)$. The interaction Hamiltonian is then reduced to $H_{\text{int}} = (e/m)\mathbf{p}\cdot\mathbf{A}(t)$. We can also write it as

$$H_{\text{int}} = -(p_{12}|1\rangle\langle 2| + p_{21}|2\rangle\langle 1|)E(t), \tag{2.6}$$

where $\mathcal{E}(t) = -\partial\mathbf{A}/\partial t$, is the laser electric field, and we have introduced the electric dipole moment of the atomic transition, as $p_{12} = p_{21}^* = -e\langle 1|(\mathbf{r}\cdot\mathbf{e})|2\rangle$, where $\mathbf{e} = \mathcal{E}/|\mathcal{E}|$ is the unit polarization vector. In the particular case of linear polarization along the x-axis, we can simply write $(\mathbf{r}\cdot\mathbf{e}) = x$.

It can easily be realized that the off-diagonal terms of the interaction Hamiltonian are $H_{12} = H_{21}^* = p_{12}E(t)$. We should also notice that the diagonal terms of this Hamiltonian are equal to zero, because they contain factors of the form $\langle 1|2\rangle = 0$. Replacing this in the evolution equations (2.4), and using an electric field of the form $\mathcal{E}(t) = \mathcal{E}_0\cos(\omega t)$, where $\mathcal{E}$ is the amplitude an ω the laser frequency, we get

$$\frac{\partial C_1}{\partial t} = -i\,\Omega_R e^{-i\,\omega_0 t}\cos(\omega t)C_2, \quad \frac{\partial C_2}{\partial t} = -i\,\Omega_R^* e^{i\,\omega_0 t}\cos(\omega t)C_1, \tag{2.7}$$

where the new quantity $\Omega_R = p_{12}E_0/\hbar$ is called the *Rabi frequency*. The solutions of these coupled equations are well known. First, we consider the case of an atom which is initially in the lower energy level $|1\rangle$, and is submitted to a low intensity laser field. This means that coupling with the excited state $|2\rangle$ ia weak, and we can take $C_1(t) \simeq 1$, leading to the simple solution

$$C_2(t) = \frac{1}{2}\Omega_R^*\left[\frac{1-e^{i(\omega_0+\omega)t}}{(\omega_0+\omega)} + \frac{1-e^{i(\omega_0-\omega)t}}{(\omega_0-\omega)}\right]. \tag{2.8}$$

The transition probability from the lower to the upper state is $|C_2(t)|^2$. For long interaction times, the second term in this equation becomes dominant, and we can approximately write

$$|C_2(t)|^2 \simeq \frac{|\Omega_R|^2}{4}\left|\frac{1-e^{i(\omega_0-\omega)t}}{(\omega_0-\omega)}\right|^2 = |\Omega_R|^2\,\frac{\sin^2[(\omega_0-\omega)t/2]}{(\omega_0-\omega)^2}. \tag{2.9}$$

The neglection of the non-resonant term is known as the *rotating wave approximation*. The transition probability attains a maximum at resonance, when $\omega = \omega_0$, with a value that evolves proportional to the square of time $|C_2(t)|^2 = \frac{1}{4}|\Omega_R|^2 t^2$. A more general solution can be obtained in the rotating wave approximation, where the coupled equations (2.7) reduce to

$$\frac{\partial C_1}{\partial t} = -\frac{i}{2}\Omega_R e^{-i\,\Delta t}C_2, \quad \frac{\partial C_2}{\partial t} = -\frac{i}{2}\Omega_R^* e^{i\,\Delta t}C_1, \tag{2.10}$$

where $\Delta = \omega_0 - \omega$ is the frequency detuning. Solving this we get

$$|C_2(t)|^2 = \frac{|\Omega_R|^2}{\Omega^2} \sin^2\left(\frac{t}{2}\Omega\right). \tag{2.11}$$

This shows that the occupation of the energy levels oscillates with a frequency $\Omega = \sqrt{|\Omega_R|^2 + \Delta^2}$. In the resonant case of $\omega = \omega_0$, or $\Delta = 0$, we are reduced to $\Omega = |\Omega_R|$. This shows that the Rabi frequency $|\Omega_R|$ is the natural frequency of oscillation of the energy level occupation probability, at resonance. In this case, the above expression reduces to $|C_2(t)|^2_{\Delta=0} = \sin^2(|\Omega_R|t/2)$. This means that the occupation probability attains its maximum value after multiples of the time interval $\Delta t = \pi/2|\Omega_R|$. Noting that $|C_1(t)|^2 + |C_2(t)|^2 = 1$, we conclude that the occupation probability oscillated between the two states of the atomic transition, and that, on the average, its occupation is $1/2$ for both states. These qualitative features are confirmed by a full quantum description (see the Appendix).

Another important aspect of the atom laser interaction is the existence of an energy shift of the lower energy level. This can be determined in the following way. The use of Eq. (2.8) on the first of Eq. (2.7) leads to the following result

$$\left\langle \frac{\partial C_1}{\partial t} \right\rangle = -\frac{i}{4}|\Omega_R|^2 \left[\frac{1}{(\omega_0 + \omega)} + \frac{1}{(\omega_0 - \omega)} \right], \tag{2.12}$$

where the simbol $\langle \cdot \rangle$ represents here a time average taken over one cycle of the radiation field. For non-resonant transitions $\omega \neq \omega_0$, we can identify this quantity with the average energy shift of the ground energy level, $\Delta E = i\hbar\langle dC_1/dt \rangle$, which leads to

$$\Delta E = \hbar|\Omega_R|^2 \frac{\omega_0}{(\omega_0^2 - \omega^2)}. \tag{2.13}$$

If we take into account all the possible non-resonant radiative transitions, from several energy levels $|j\rangle$ to the same ground state, we can generalize it to

$$\Delta E = \mathcal{E}_0^2 \sum_j \frac{|p_{j1}|^2 \omega_{j1}}{(\omega_j^2 - \omega^2)}, \tag{2.14}$$

where $\mathcal{E}_0$ is the amplitude of the laser electric field, $\omega_{j1} = (E_j - E_1)/\hbar$ the different atomic transition frequencies and p_{j1} the corresponding electric dipole moments. We should notice that, in the zero frequency limit, $\omega \to 0$, this reduces to the well known Stark shift due to a static electric field. For this reason, the energy shifts described by Eqs. (2.13) or (2.14) are usually called the *ac Stark effect*.

It is sometimes useful to describe the Rabi oscillations in terms of the *density matrix operator*, which can be defined as $\rho = |\psi\rangle\langle\psi|$. For a two-level atom model, such that $|\psi| = C_1(t)|1\rangle + C_2(t)|2\rangle$, the diagonal matrix elements are

$$\rho_{11} = \langle 1|\rho|1\rangle = |C_1(t)|^2, \quad \rho_{22} = \langle 2|\rho|2\rangle = |C_2(t)|^2 \tag{2.15}$$

and the off-diagonal terms

$$\rho_{12} = \langle 1|\rho|2\rangle = C_1(t)C_2^*(t), \quad \rho_{21} = \rho_{12}^*. \tag{2.16}$$

We can see that the diagonal terms are real quantities and their sum equal to one, $\rho_{11} + \rho_{22} = 1$. We can also see that, for a collection of identical N atoms per unit volume, there will be a population of atoms in the lower state $N_1(t)$, and a population in the upper state $N_2(t)$, such $\rho_{11} = N_1(t)/N$, and $\rho_{22} = N_2(t)/N$. The temporal evolution of the density matrix elements can be derived from the above equations for the coefficients $C_j(t)$ and, in the rotating wave approximation, we get

$$\frac{d\rho_{11}}{dt} = -\frac{d\rho_{22}}{dt} = \frac{i}{2}\Omega_R^* e^{-i\Delta t}\rho_{12} - \frac{i}{2}\Omega_R e^{i\Delta t}\rho_{21} \tag{2.17}$$

and

$$\frac{d\rho_{12}}{dt} = \frac{d\rho_{21}^*}{dt} = i\,\Omega_R e^{i\Delta t}(\rho_{11} - \rho_{22}). \tag{2.18}$$

These are known as the *optical Bloch equations*. The original Bloch equations, which are formally identical, were derived to describe the spin states in a magnetic field. The interest of this new formulation in terms of the density matrix elements is that it can easily be extended to a mixed state, such that $\rho = \sum_j p_j|\psi_j\rangle\langle\psi_j|$, where p_j are the probabilities for the quantum system to be in a state $|\psi_j\rangle$. For initial conditions $\rho_{11}(0) = 1$ and $\rho_{22}(0) = \rho_{12}(0) = 0$, we get the solutions (2.11) for $\rho_{22}(t)$, and

$$\rho_{12}(t) = \frac{|\Omega_R|^2}{\Omega^2}\sin\left(\frac{\Omega t}{2}\right)\left[i\,\Omega\cos\left(\frac{\Omega t}{2}\right) - \Delta\sin\left(\frac{\Omega t}{2}\right)\right]e^{-i\Delta t}. \tag{2.19}$$

Although spontaneous emission is not described in the frame of the present semi-classical approach to the atom-laser interaction, we can include it by adding a phenomenological term into the above evolution equations. Defining Γ as the spontaneous decay rate of the upper energy level, the above Eqs. (2.17) and (2.18) become

$$\frac{d\rho_{11}}{dt} = -\frac{d\rho_{22}}{dt} = \Gamma\rho_{11} + \frac{i}{2}|\Omega_R|\,(\tilde{\rho}_{12} - \tilde{\rho}_{21}) \tag{2.20}$$

and

$$\frac{d\tilde{\rho}_{12}}{dt} = \frac{d\tilde{\rho}_{21}^*}{dt} = i\,|\Omega_R|(\rho_{11} - \rho_{22}) - (\Gamma/2 + i\,\Delta)\tilde{\rho}_{12}, \tag{2.21}$$

where we have used $\tilde{\rho}_{12} = \rho_{12}\exp(-i\,\Delta t - i\,\varphi)$, where φ is the phase of the Rabi frequency, $\Omega_R = |\Omega_R|\exp(i\,\varphi)$. Steady state solutions of these equations will be an important ingredient of the laser cooling precess, as discussed next.

2.2 Laser Cooling Force

The process of atom cooling by laser radiation can be very easily understood with the help of two complementary pictures: the energy and the momentum pictures, which are illustrated in Fig. 2.1. The energy picture can be described in the following way. Assume an atom with two internal energy states, with energies E_1 and E_2, interacting with a slightly red-tuned radiation field with frequency $\omega < \omega_0 \equiv (E_2 - E_1)/\hbar$, and wave vector $\mathbf{k}$. Resonant radiative transition from the lower to the upper energy level, $|1\rangle \rightarrow |2\rangle$, can occur by photon absorption if the atom moves with velocity $\mathbf{v}$, such that the Doppler shifted photon frequency becomes equal the transition frequency, $(\omega - \mathbf{k} \cdot \mathbf{v}) = \omega_0$.

If then the upper energy level spontaneously decays, by photon emission in a direction perpendicular to the atom velocity, the radiation field will gain an energy of $\hbar|\mathbf{k} \cdot \mathbf{v}|$, and due to energy conservation, the atom will loose the same amount of kinetic energy, given that it returns to the initial internal energy state $|1\rangle$. If the fluorescence lifetime of the upper state $|2\rangle$ is short, such a cycle of "photon absorption followed by radiative decay" can repeat several times in a second, the kinetic energy of the atom will reduce on the average and the atom will slow down, leading to a significant gas cooling.

Let us now consider the more commonly used momentum picture, which describes the same absorption-emission cycle from a different perspective. Due to momentum conservation, when an atom emits one photon with frequency ω and wavevector $\mathbf{k}$, it acquires a momentum $-\hbar\mathbf{k}$, which is called the *momentum recoil*. Inversely, when an atom absorbs a photon, it will absorb the photon momentum $\hbar\mathbf{k} \equiv \hbar k\mathbf{n}$, where $\mathbf{n}$ is the unit vector along the direction of $\mathbf{k}$. If such an absorption

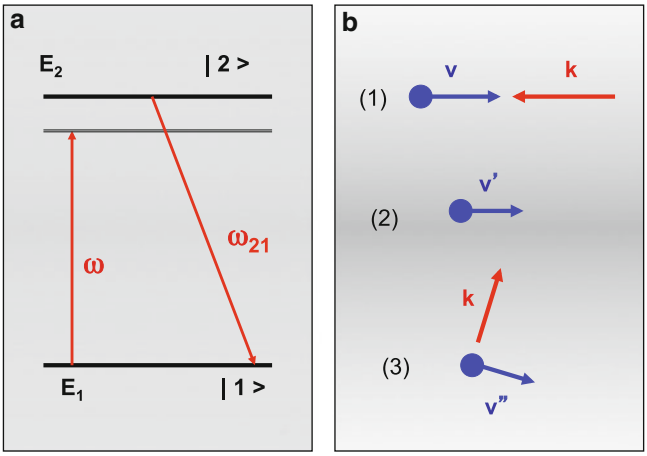

Fig. 2.1 Basic absorption-emission cycle of atomic laser cooling: two complementary pictures. (**a**) Energy picture, with a virtual energy level $E_2 - |\mathbf{k} \cdot \mathbf{v}|$; (**b**) Momentum picture, with an intermediate atom velocity $v' = v - \hbar k/M$

is followed by spontaneous emission at the same frequency $\omega = k/c$, the emitted photon will propagate in an arbitrary direction defined by $\mathbf{n}' = \mathbf{k}'/k$. As a result, in the emission-absorption cycle the atom translational momentum is not conserved, and it will receive a net momentum given by $\Delta\mathbf{p} = \hbar(\mathbf{k} - \mathbf{k}') = \hbar\omega(\mathbf{n} - \mathbf{n}')/c$. If such a cycle is repeated many times by the same atom, the momentum loss by spontaneous emission will be averaged to zero and a net momentum gain will be obtained. We can write the total momentum balance after r successive cycles of absorption-emission processes, as

$$\Delta\mathbf{P} = r\left(\hbar\mathbf{k} - \hbar\sum_{j=1}^{r}\mathbf{k}'_j\right). \tag{2.22}$$

Taking the average for a large number $r \gg 1$, the last term averages to zero, and we are reduced to $\langle\Delta\mathbf{P}\rangle \simeq r\hbar\mathbf{k}$. If r is the fluorescence rate, we can define the *ponderomotive force* acting on the atom (the momentum variation per unit time) as

$$\mathbf{F}_p = r\hbar\mathbf{k}. \tag{2.23}$$

It is obvious that this fluorescence rate is determined by the product of the spontaneous decay rate Γ with the upper energy level population of the atom, or $r = \Gamma\rho_{22}$. Let us go back to the evolution equations for the density matrix elements, describing the radiation coupling between the two energy levels $|1\rangle$ and $|2\rangle$, as given by (2.20) and (2.21). In steady state, $d/dt = 0$, these equations yield

$$\tilde{\rho}_{22} = -\frac{i}{2\Gamma}\Omega_R(\tilde{\rho}_{21} - \tilde{\rho}_{12}), \quad \tilde{\rho}_{12} = -i\frac{\Omega_R}{2}\frac{2\tilde{\rho}_{22} + 1}{(i\Delta - \Gamma/2)} = \tilde{\rho}^*_{21}, \tag{2.24}$$

with $\tilde{\rho}_{ij}$ standing for the steady-state values of the matrix elements ρ_{ij}. Using this result in Eq. (2.23), we can then write the ponderomotive force of the incident laser beam on the atom as

$$\mathbf{F}_p = \hbar\mathbf{k}\Gamma\tilde{\rho}_{22} = \hbar\mathbf{k}\Gamma\frac{\Omega_R^2}{2\Omega_R^2 + 4\Delta^2 + \Gamma^2}. \tag{2.25}$$

This result is valid for an atom at rest in the laboratory frame, or if the atom is moving, in the atom frame. We can now explicitly introduce the motion of the atom in the expression of the ponderomotive force. As noticed before, due to the Doppler effect, the laser photons are perceived as having a shifted frequency $\omega' = \omega - \mathbf{k}\cdot\mathbf{v}$. This introduces an additional detuning with respect to the transition frequency ω_0. The resulting expression for the force acting on the moving atom will then be

$$\mathbf{F}_p = \hbar\mathbf{k}\Gamma\frac{\Omega_R^2}{4(\Delta + \mathbf{k}\cdot\mathbf{v})^2 + \Gamma^2 + 2\Omega_R^2}. \tag{2.26}$$

For low intensities such that the radiative transition is not saturated, $\Omega_R^2 \ll \Gamma^2/2$, we can neglect the Rabi frequency in the denominator of the force. Using the following approximation

$$\frac{1}{4(\Delta + \mathbf{k}\cdot\mathbf{v})^2 + \Gamma^2} \simeq \frac{1}{(4\Delta^2 + \Gamma^2) + 8(\mathbf{k}\cdot\mathbf{v})\Delta} \simeq \frac{1}{(4\Delta^2 + \Gamma^2)}\left[1 - \frac{8\Delta(\mathbf{k}\cdot\mathbf{v})}{(4\Delta^2 + \Gamma^2)}\right], \tag{2.27}$$

the force acting on the atom can be approximately determined by

$$\mathbf{F}_p = \mathbf{F}_0 - \frac{M\beta\mathbf{k}}{2k^2}\mathbf{k}\cdot\mathbf{v}, \tag{2.28}$$

where M is the atomic mass, and

$$\mathbf{F}_0 = \hbar\mathbf{k}\Gamma\frac{\Omega_R^2}{(4\Delta^2 + \Gamma^2)}, \quad \beta = \hbar\Gamma k^2\frac{2^4\Omega_R^2\Delta}{M(\Delta^2 + \Gamma^2/4)}. \tag{2.29}$$

Let us consider the particularly interesting case when the atom moves in the direction of the laser propagation, $\mathbf{k} \parallel \mathbf{v}$. We are then reduced to

$$\mathbf{F}_p = \mathbf{F}_0 \mp \frac{1}{2}\beta M\mathbf{v}. \tag{2.30}$$

We can then see that two different terms occur in the ponderomotive force $\mathbf{F}_p$. The first term, $\mathbf{F}_0$, is a constant radiation pressure term, which is independent of the atom velocity. In contrast, the second term can be seen as a friction term which depends on the atom velocity. It is positive for an atom moving in the opposite direction with respect to the laser beam (the atom slows down), and negative for an atom moving along the beam (the atom is pushed forward). If now the atom is located in a region with two opposite laser beams, and moves along the laser beam axis, it will experiment a total force in the $\mathbf{k}$ direction as given by

$$\mathbf{F}_p = \left(\mathbf{F}_0 - \frac{\beta}{2}M\mathbf{v}\right) - \left(\mathbf{F}_0 + \frac{\beta}{2}M\mathbf{v}\right) = -\beta M\mathbf{v}. \tag{2.31}$$

This shows that, with two counter-propagating beams, the pressure term is zero and the friction force is always negative, leading to a deceleration. The atom will therefore slow down along that direction. If the same occurs for every atom in the gas, the gas will then cool down. This is the laser cooling effect, which leads to extremely low temperatures in the micro-Kelvin domain, as first observed in the experiments with optical *molasses* by Chu and collaborators [4]. The term 'molasse' was coined because of the resemblance of the resulting viscous photon fluid to real molasses.

2.3 Doppler Limit

Let us now discuss the theoretical limits of this cooling process. These limits can be discussed by using a statistical approach to the spontaneous emission. For that purpose, we study the evolution of the atomic momentum distribution of the cold gas, $f(p,t)$, in a one-dimensional description. This evolution is determined by a Fokker-Planck equation of the form

$$\frac{\partial}{\partial t} f(p,t) = \frac{\partial}{\partial p}\left[A(p) + D(p)\frac{\partial}{\partial p}\right] f(p,t), \tag{2.32}$$

where $A(p)$ and $D(p)$ are the friction and diffusion coefficients. A steady state solution of this equation is given by

$$f(p) = f_0 \exp\left[-\int_0^p \frac{A(p')}{D(p')} dp'\right], \tag{2.33}$$

We know that the friction coefficient is related to the averaged particle momentum by $d\langle p\rangle/dt = -A(p)$. Comparing with the results obtained in the previous section, we can write the following relation

$$A(p) = \beta M v = \beta p = 8\hbar k^2 \Gamma \Delta \frac{\Omega_R^2}{M(4\Delta^2 + \Gamma^2))^2}. \tag{2.34}$$

Noting that, in typical experimental situations we have $\Omega_R \sim \Delta \sim \Gamma$, we can, for the sake of magnitude estimates, use a much simpler expression, $A(p) \sim \hbar k^2 p/M$. Turning now to the diffusion coefficient $D(p)$, we know that by definition, it is given by

$$D(p) = \frac{1}{2}\frac{\langle \Delta p\rangle^2}{\Delta t} \sim \frac{1}{4}\hbar^2 k^2 \Gamma \tag{2.35}$$

The integration of the steady state solution (2.33) then leads to

$$\int_0^p \frac{A(p')}{D(p')} dp' \simeq \int_0^p \frac{\hbar k^2 p'}{M} \frac{4}{\hbar^2 k^2 \Gamma} dp' = \frac{2}{M\Gamma} p^2 \tag{2.36}$$

We can then reduce the steady state distribution $f(p)$ to a Maxwell distribution such that

$$f(p) = f_0 \exp\left(-\frac{p^2}{2M T_D}\right) \tag{2.37}$$

with the effective temperature (in energy units)

$$T_D \sim \frac{\hbar}{2}\Gamma, \tag{2.38}$$

known as the *Doppler temperature* limit. We can see that this temperature is limited by the natural life-time of the atomic transition. This result has a simple physical meaning. We note that the spontaneous emission implies a time uncertainty of $\Delta t \sim 1/\Gamma$. Therefore, according to the uncertainty principle, the energy uncertainty is of order $\Delta E \sim \hbar\Gamma$ which nearly coincides with (2.38). For a detailed discussion of the Doppler limit see [5].

2.4 Magnetic Traps

Atoms can be confined by static magnetic fields, by oscillating fields and by laser light. Confinement of neutral atoms in static magnetic traps is a well established technique, first reported by Migdall et al. [6]. In recent years, this technique has evolved into the fabrication of atomic chips at the micro-meter scale, using several magnetic trap configurations [7]. It is well known that magnetic fields produce an energy shift in the internal atomic levels. For inhomogeneous magnetic fields, this leads to the occurrence of local energy minima where the atoms can be confined. For an atom with a permanent magnetic moment μ, at rest in a static magnetic field $\mathbf{B}$, the energy shift can be defined as

$$\Delta E(\mathbf{r}) = -\mu \cdot \mathbf{B}(\mathbf{r}) = g_J \mu_B m_J |\mathbf{B}(\mathbf{r})| \tag{2.39}$$

where m_J is the projection of the total angular momentum $\mathbf{J}$, g_J is the corresponding Landé factor, and $\mu_B = e\hbar/2m_e$ is the *Bohr magneton*. A well known general theorem prevents the occurrence of static magnetic field maxima in free space, in the absence of currents. This means that only local minima can be created in the experiments. For atomic states such that $g_J m_J > 0$, this interaction allows to create energy minima around which the atoms can be confined. If the atom is moving with velocity $\mathbf{v}$, it will perceive a time varying magnetic field, which can eventually induce transitions between these magnetic states, thus allowing a trapped atom to become untrapped. According to Eq. (2.39), the typical energy difference between magnetic states is $\hbar\omega_L$, where $\omega_L = |\mu B|/\hbar$ is the *Larmor frequency*. The time scale for field variation in the atom rest frame is determined by $dB/dt = \mathbf{v} \cdot \nabla B$. If this time scale remains much larger than $1/\omega_L$ the magnetic dipole of the atom will have time to adapt to the slowly varying field, and the atom will stay in the same magnetic state. Therefore, the existence of such an *adiabatic regime* will be defined by the inequality

$$\frac{1}{B}\frac{dB}{dt} \ll \omega_L. \tag{2.40}$$

If, at some given position this inequality is not verified, transitions to other magnetic states can take place, which means that magnetic confinement can fail. This is the case, in particular for regions where the magnetic field amplitude, and the Larmor

frequency, tend to zero. This is the reason why the magnetic minimum of a magnetic trap cannot be zero. A non-zero minimum has to exist in other to fulfill the adiabatic condition at the centre of the trap.

2.4.1 Multipolar Field Configuration

Simple magnetic configurations with a magnetic field minimum can be constructed, using the basic elements of conducting currents, straight wires and coils. Let us first consider the *multipolar field* configuration produced by a number n of linear and parallel conductors, with the same current I flowing all of them in the same direction. The conductors are assumed over an imaginary cylindrical surface with radius a, and parallel to the axis of the cylinder, and can be described by the current density $\mathbf{J}(\mathbf{r}) = \sum_{j=1}^{n} I\,\mathbf{e}_z \delta(\mathbf{r} - \mathbf{r}_j)$, where $\mathbf{r}_j$ is a polar vector with components $x_j = a\cos(2\pi j/n)$ and $y_j = a\sin(2\pi j/n)$. The corresponding vector potential $\mathbf{A}$ can be written as

$$\mathbf{A} = -\frac{\mu_0 I}{4\pi}\mathbf{e}_z \ln R\ , \quad R^2 = \Pi_{j=1}^{n} r_j^2 = \left(a^{2n} + r^{2n} - 2r^n a^n \cos n\theta\right) \tag{2.41}$$

In the inner region, close to the cylindrical axis where $r \ll a$, the resulting magnetic field $\mathbf{B} = \nabla \times \mathbf{A}$ can be written in polar coordinates as

$$B_r \simeq -n\frac{\mu_0 I}{2\pi a}\left(\frac{r}{a}\right)^{n-1} \sin(n\theta)\ , \quad B_\theta \simeq -n\frac{\mu_0 I}{2\pi a}\left(\frac{r}{a}\right)^{n-1} \cos(n\theta) \tag{2.42}$$

From here we conclude that the magnetic field tends to zero when we approach the cylindrical axis, with a field strength varying with distance as

$$B = \sqrt{B_r^2 + B_\theta^2} \simeq n\frac{\mu_0 I}{2\pi a}\left(\frac{r}{a}\right)^{n-1}. \tag{2.43}$$

This result shows that B increases in the radial direction. In this sense it can be considered a *minimum B* configuration. It is also possible to consider a similar multipolar field produced by $2n$ parallel conductors, where alternatively the current reverses its direction. This means that, we will have a current I along the z-axis, for straight wires located on the same imaginary cylindrical surface at $r = a$ and $\theta = 2\pi j/n$, for $j = 1, 2, \ldots n$, and a current $-I$ for the remaining n wires located at $r = a$ and $\theta = (2j + 1)\pi/n$, for $j = 1, 2, \ldots n$. The resulting vector potential is now determined by

$$\mathbf{A} = -\frac{\mu_0 I}{4\pi}\mathbf{e}_z \ln\left(\frac{R_-}{R_+}\right)\ , \quad R_\pm^2 = \Pi_{j=1}^{n} r_j^2 = \left(a^{2n} + r^{2n} \pm 2r^n a^n \cos n\theta\right) \tag{2.44}$$

In the region close to the cylindrical axis, $r \ll a$, the magnetic field is approximately given by twice the previous value in Eq. (2.43), which results from the fact that we have twice as much wires. In this sense, there is no significant change for the field near the axis, if we revert the current alternatively in half of them. We still get a minimum field configuration. However, the same is not true for $r \sim a$ where significant field changes will occur.

2.4.2 Helmholtz Configuration

Another simple magnetic configuration is produced by two parallel coils, with radius a, located at a distance $2l$ from each other, at $z = \pm l$. We consider the case where the currents in the two coils are equal to I and flow in the same direction. The resulting vector potential is purely poloidal, and determined by the expression

$$A_\theta \simeq \frac{\mu_0 I a^2}{(a^2 + l^2)^{3/2}} r \left[1 + \frac{15}{2} \frac{l^2 z^2}{(a^2 + l^2)^2}\right]. \tag{2.45}$$

This field configuration now exhibits a minimum at $z = 0$, which in contrast with the multipolar configuration is not zero. A closer analysis shows that this minimum only exists for $a < 2l$. In the opposite case, the minimum is replaced by a maximum at $z = 0$. The corresponding magnetic field close to the magnetic axis $r \ll a$ is purely axial, $B_r \sim 0$ and $B_\theta \sim 0$, with a minimum given by

$$|B_z|_{\min} \simeq \frac{\mu_0 I a^2}{(a^2 + l^2)^{3/2}}. \tag{2.46}$$

On the other hand, the field will be maximum near the coils, at $z = \pm l$. Quite often, we characterize the magnetic mirror by the ratio $R = |B_z|_{\max}/|B_z|_{\min}$. This configuration is known as a simple *magnetic mirror*. It can easily be recognized that the two configurations discussed above are in some sense complementary, because near the origin, the field increases radially in the multipolar case, and axially in the magnetic mirror.

2.4.3 Ioffe Configuration

A superposition of the two basic configurations was first proposed by Ioffe for plasma confinement [8], and latter applied to neutral atoms [9]. This is called a *Ioffe trap* and it is able to created a local minimum at the origin. The resulting field can be described by

$$B(z, r) = B_0 + \frac{r^2}{2}\left(\frac{B_1^2}{B_0} - B_2\right) + B_2 z^2, \tag{2.47}$$

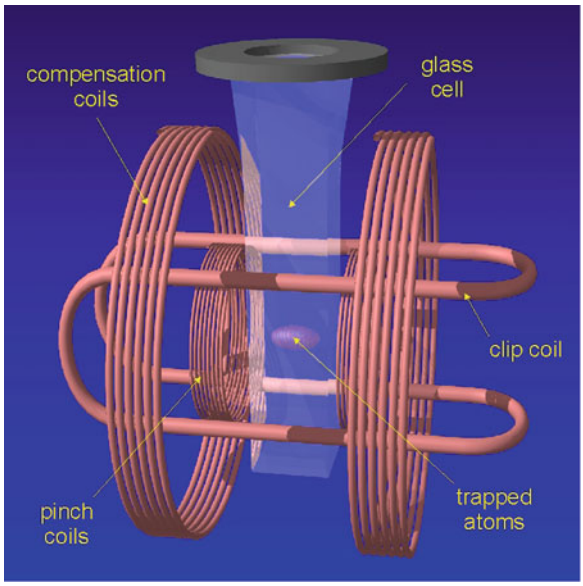

Fig. 2.2 A magnetic trap with Ioffe configuration. For experimental purposes, two compensation coils are used to control the bias field B_0

where B_0, B_1 and B_2 are positive constants. The field is minimum on axis ($z = 0$) if $B_1^2 > B_0 B_2$. The quantity B_0 is usually referred as the *bias field*, and gives the magnetic field minimum at the centre of the trap. Atoms with temperature T can be trapped if $\mu_J B_0 \gg T$. The trapping potential seen by an atom of mass M can then be written as

$$V(\mathbf{r}) = \frac{1}{2} M \omega_z^2 z^2 + \frac{1}{2} \omega_r^2 r^2, \tag{2.48}$$

where ω_z and ω_r are the axial and radial oscillating frequencies, as determined by

$$\omega_z = \sqrt{|\mu| \left(\frac{B_1^2}{B_0} - B_2 \right) / M}\ , \quad \omega_r = \sqrt{|\mu| B_2 / M}. \tag{2.49}$$

The Ioffe trap configuration is topologically equivalent to a *baseball* coil, as illustrated in Fig. 2.2, where the pinch and clip coils create the basic magnetic configuration.

2.4.4 Anti-Helmholtz Configuration

One of the simplest ways to produce a magnetic minimum is to revert the currents in the simple magnetic mirror. When the currents are equal in the coils, but flow in opposite directions, the vector potential (2.45) is replaced by

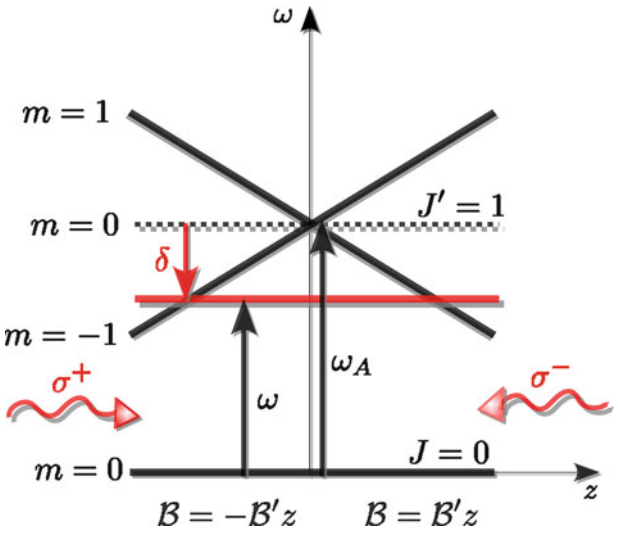

Fig. 2.3 Schematic representation trapping mechanism in one dimension MOT for a $J = 0 \rightarrow J' = 1$ transition in an atom

$$A_\theta \simeq -A_0 r z\,, \quad A_0 = 3\left(\mu_0 I a^2\right) \frac{l}{(a^2 + l^2)^{5/2}}. \tag{2.50}$$

This is again valid for the region $r \ll a$. The corresponding magnetic field has components $B_\theta = 0$, $B_r = A_0 r$ and $B_z = 2A_0 z$. And the total field strength in the vicinity of the origin is determined by

$$B(\mathbf{r}) = A_0 \sqrt{r^2 + 4z^2}. \tag{2.51}$$

This field satisfies a minimum criterion, and increases in all directions, but with a slope which is different for the axial and the radial directions. In the case where $a = l$ this is usually called the *anti-Helmholtz configuration*. An important difference with respect to the Ioffe trap is that the magnetic field minimum here is equal to zero, which increases the trap losses near the centre.

Let us finally consider a magneto-optical trap (MOT) which results from the simultaneous use of laser cooling beams and a magnetic trapping, or from an atomic physics perspective, a combination of Zeeman and Doppler shifts. The magnetic configuration is basically made of two anti-Helmholtz coils as discussed above.

In order to describe the principle of a magneto-optical trap, we consider an atom ground state, with total angular momentum $J = 0$, and an excited state with angular quantum number $J = 1$, with three sub-levels $m_J = 0, \pm 1$. Two counter-propagating laser beams are red-detuned with respect to the atomic transition, with left and right circular polarizations $\sigma^{\pm}$. The inhomogeneous magnetic field created by the two anti-Helmholtz coils is zero at the centre of the trap and increases linearly, as shown in Fig. 2.3. The laser beam with polarization σ^+ (propagating

along the negative z-direction in this figure) can couple the ground state to the $m = +1$ excited state, due to the additional Doppler shift associated with atoms moving outwards in the positive region $z > 0$. A similar process occurs with the atoms moving outwards in the region $z < 0$, with transitions allowed to the state $m = -1$ by the laser beam with polarization σ^-. The net result is cooling and radiative pressure pushing the atoms towards the centre of the trap, $z = 0$. Minimal temperature is attained for a detuning of the order of $\Delta = (\Gamma/2)\sqrt{1 + I/I_{\text{sat}}}$, where Γ is the atomic transition line width, I is the laser intensity and I_{sat} the saturation intensity. In typical experimental conditions, we can choose $I/I_{\text{sat}} \sim 10 - 100$, which corresponds to $\Delta \sim (1 - 10)\Gamma$. This is obviously much larger than the requirement for attaining the Doppler limit temperature, and indeed temperatures well below this limit are obtained. This is due to the existence of additional cooling processes that can take place in a MOT, as those described next.

The magneto-optical trap was first experimentally used by Raab et al. [10] and now became a common technique for the production and confinement of an ultra-cold gas. In such a device, the laser and magnetic confinement forces considered so far are complemented by collective forces, resulting from long range atomic interactions, which will be discussed later in Chap. 4.

2.5 Sisyphus Cooling

The limitations of the Doppler cooling theory, based on the two-level atom configuration, became rather evident as experiments performed with optical molasses soon revealed that the temperatures were actually much lower than the limit given in Sect. 2.3. This happens because two important ingredients were ignored within the simple Doppler cooling theory: first, the intensity of the radiation field produced by two counter-propagating lasers is inhomogeneous; second, real atoms are not two-level systems; in fact, they have Zeeman sub-levels in the ground state.[1] The physics behind cooling in this configuration is, however, rather involved [11], for which we draw some of the most important lines here.

Let us consider an atom interacting with two counter-propagating laser beams, along the z axis, possessing the same frequency ω_0 but in orthogonal polarization states, such that

$$\mathbf{E}(\mathbf{r}, t) = E_0 \left(\mathbf{e}_1 e^{i\mathbf{k}_0\cdot\mathbf{r}} + \mathbf{e}_2 e^{-i\mathbf{k}_0\cdot\mathbf{r}}\right) e^{-i\omega_0 t} + \text{c.c.}, \tag{2.52}$$

with $(\mathbf{e}_1 \cdot \mathbf{e}_2) = 0$, and $(\mathbf{e}_1 \cdot \mathbf{k}_0) = (\mathbf{e}_2 \cdot \mathbf{k}_0) = 0$. For instance, we can set $\mathbf{k}_0 = k_0\mathbf{e}_z$ and $\mathbf{e}_1 = \mathbf{e}_x$ and $\mathbf{e}_2 = \mathbf{e}_y$. This is equivalent to write

$$\mathbf{E}(\mathbf{r}, t) = \sqrt{2}E_0\mathbf{e}(\mathbf{r})e^{i\mathbf{k}_0\cdot\mathbf{r} - i\omega_0 t} + \text{c.c.}, \tag{2.53}$$

[1] Actually, in the absence of magnetic fields, alkali atoms have degenerate ground states.

where $\mathbf{e}(\mathbf{r})$ is a position dependent unit polarization vector, as defined by

$$\mathbf{e}(\mathbf{r}) = \frac{1}{\sqrt{2}}\left(\mathbf{e}_1 + \mathbf{e}_2 e^{-2i\mathbf{k}_0\cdot\mathbf{r}}\right). \tag{2.54}$$

This shows that the field polarization changes along the z-direction with a period of $\pi/k_0 = \lambda_0/2$, half the laser wavelength, alternating between linear and circular polarization. Such an alternation can be shown more explicitly by introducing the right and left circular polarization vectors, $\mathbf{e}_\pm = (\mathbf{e}_1 \pm i\,\mathbf{e}_2)/\sqrt{2}$, in terms of which the above expression becomes

$$\mathbf{e}(\mathbf{r}) = \frac{1}{2}\mathbf{e}_+\left[1 - \sin(2\mathbf{k}_0\cdot\mathbf{r})\right] + \frac{1}{2}\mathbf{e}_-\left[1 + \sin(2\mathbf{k}_0\cdot\mathbf{r})\right] + \frac{1}{\sqrt{2}}\mathbf{e}_2\cos(2\mathbf{k}_0\cdot\mathbf{r}). \tag{2.55}$$

This shows that the intensity of the right and left circular polarization modes vary in space as

$$I_\pm \propto \frac{1}{2}\left[1 \mp \sin(2\mathbf{k}_0\cdot\mathbf{r})\right]. \tag{2.56}$$

For a ground state with two degenerate magnetic quantum numbers $m_g = \pm 1/2$, this can lead to an energy shift of the ground states $g = \pm 1/2$, due to the existence of these $\sigma^\pm$ polarization modes, of the form

$$\Delta E^\pm = -U_0\left[1 \mp \sin(2\mathbf{k}_0\cdot\mathbf{r})\right], \quad \text{with} \quad U_0 = \frac{\hbar\Omega_R^2\Delta}{\Gamma^2 + 4\Delta^2}. \tag{2.57}$$

An atom moving to the right ($\mathbf{k}_0$ positive direction) in the state $m_g = +1/2$, will be excited to the upper level by the σ^+ polarization mode, near the upper part of the oscillating potential hill (see Fig. 2.4). It will then be optically pumped to the other ground sub-level at the bottom of the well, by emitting a blue shifted photon. The kinetic energy loss will therefore be of the order of U_0. This process will then repeat itself, with more probability for an atom to climb the potential hill than to go down.

The lowest temperature limit is now given by the recoil energy associated with the process of photon emission by a atom. This recoil energy is $E_{\rm rec} = (\hbar k)^2/2M$, where $\hbar k \simeq \hbar\omega_0/c$ is the photon momentum, and M the mass of the atom. The resulting *recoil temperature* limit, $T_{\rm rec}$ is given in energy units by

$$T_{\rm rec} \equiv E_{\rm rec} = \frac{\hbar^2\omega_0^2}{2Mc^2}. \tag{2.58}$$

This value lies well below the Doppler limit, as observed in the experiments [12]. Additional cooling, leading to temperatures even lower than $T_{\rm rec}$ can be achieved with the evaporative cooling technique, which consists of extracting atoms in high kinetic energy from the trap, as discussed next. In Table 2.1, we present some of its values, together with other parameters, for the most important atomic isotopes used in experiments.

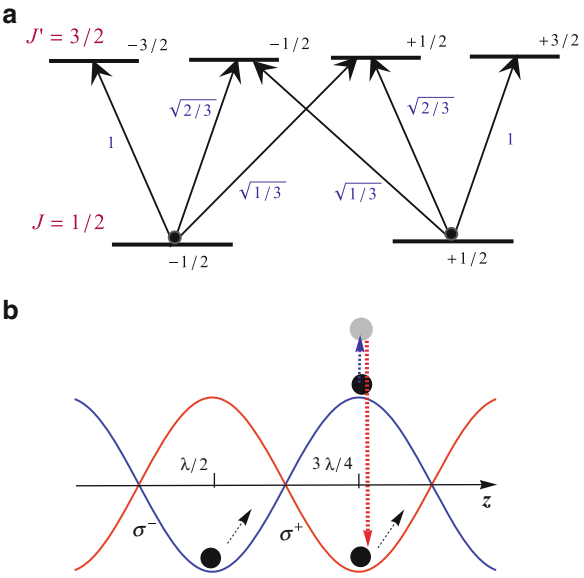

Fig. 2.4 (**a**) Schematic representation of a simple multi-level structure sensitive to the light shifts induced by the polarization gradient. (**b**) Optical pumping mechanism in an optical potential with position-dependent polarization

Table 2.1 Comparison of relevant atomic parameters for the main cooling transitions for the isotopes of elements used in laser cooling experiments. The data are taken from Ref. [13]

Isotope	Cooling transition	$\Gamma/2\pi$ (MHz)	I_s (mW/cm^2)	T_D (μK)	T_{rec} (nK)
^{39}K	$4^2S_{1/2} \rightarrow 4^2P_{3/2}$	6.2	1.81	148	830
^{87}Rb	$5^2S_{1/2} \rightarrow 5^2P_{3/2}$	5.9	1.67	145	370
^{40}Ca	$4^1S_0 \rightarrow 4^1P_1$	34.2	60	832	2,670
^{88}Sr	$4^1S_0 \rightarrow 4^1P_1$	31.8	42.7	767	1,020

2.6 Evaporative Cooling

Evaporative cooling is perceived in everyday life. It results from the fact that evaporation carries away the particles of a given body or system with the largest kinetic energies. It was first proposed to cool trapped Hydrogen atoms by Hess in 1985 [14], and later used to cool alkali atoms [15]. An early authoritative review was given in [16]. In order to produce evaporation, we need to corrode the borders of the magnetic trap in order to produce a shallow potential. This can be made by using radio-frequency fields. Given the magnetic field inhomogeneity, this field will connect upper and lower Zeeman ground levels, producing a magnetic hole that allows the atoms in the outer regions of the trap to escape. Evaporative cooling became a basic technique to attain the critical temperature and to achieve Bose Einstein condensation [17].

Let us briefly review the concepts of this cooling process, by assuming that an atomic gas is trapped inside a given potential well $U(\mathbf{r})$. The temperature drops due to loss of atoms, as characterized by the evaporation parameter α, defined as [16]

$$\alpha = \frac{d(\ln T)}{d(\ln N)}, \tag{2.59}$$

where T is the temperature and N the number of atoms. If evaporation is processed at a constant rate, then the final temperature at some later instant t can be simply determined by

$$T(t) = T(0)\left[\frac{N(t)}{N(0)}\right]^{\alpha}, \tag{2.60}$$

where $N(0)$ and $T(0)$ are the initial values. We can assume a potential well with a generic shape $U(\mathbf{r}) \propto r^{-\delta/3}$, where $\delta = 3/2$ for a three dimensional harmonic potential. Evaporation is controlled by limiting the depth U_0 of the confining potential. The kinetic energy of the escaping atoms is larger and of the order of U_0. In what concerns the trapped atoms, we can assume that they are approximately described by a Boltzmann distribution, with an average energy of $U_{\text{th}} = (\delta + 3/2)T$. Under these assumptions, it is then possible to establish a simple relation between the evaporation parameter and the potential depth, as

$$\alpha = \frac{U_0 - U_{\text{th}}}{U_{\text{th}}} = \frac{\eta}{(\delta + 3/2)} - 1, \tag{2.61}$$

where we have used $\eta = U_0/T$. We can see that, for $\eta = 6$ we have $\alpha = 1$ for a harmonic trap. A drop of temperature of 10^{-3} would then be achieved for a fraction of 10^{-3} atoms remaining inside the trap after evaporation. This would bridge the gap between the temperature range provided by laser cooling and the critical temperature required for Bose Einstein condensation, as demonstrated experimentally for alkaline atoms and for atomic Hydrogen.

Let us now consider the temporal evolution of the trapped atoms. The velocity of atoms of critical kinetic energy equal to $U_0 \equiv \eta T$, is equal to $\sqrt{2U_0/m} = \sqrt{\pi\eta}\bar{v}/2$, where $\bar{v}$ is the average velocity of the trapped atoms. For large values of η, the fraction of atoms with energies larger than the threshold U_0 is approximately given by $2e^{-\eta}\sqrt{\eta/\pi}$. From here we conclude that the rate of evaporation provided by collisions is

$$\frac{dN}{dt} = -\frac{N}{\tau_v}, \quad \tau_v = \frac{\sqrt{2}e^{\eta}}{\eta}\tau_{\text{col}}, \tag{2.62}$$

where τ_v is the evaporation time. We have also defined the elastic collision time $\tau_{\text{col}} = 1/(\sqrt{2}n_0\sigma\bar{v})$, where n_0 is the maximum density of atoms, σ is the cross section for elastic collisions, and $\sqrt{2}\bar{v}$ is the average relative velocity between two colliding atoms. This expression for the atom evaporation rate is confirmed by a more detailed analysis.

Because evaporative cooling is essentially a classical process, many classical models have been proposed [15, 18–23]. Such a classical description is valid if the temperature of the gas is much larger than the quantum level spacing of the

atoms in the trap. In addition, the de Broglie wavelength has to be larger than the mean interatomic distance, or $n\lambda_T^3 \gg 1$, where n is the atom density and $\lambda_T = \hbar\sqrt{2\pi/MT}$ is the de Broglie wavelength of a thermal atom. Following [23], let us assume a classical distribution function $f(\mathbf{r}, \mathbf{p})$, normalized to the total number of atoms in the trap, as

$$\int d\mathbf{r} \int \frac{d\mathbf{p}}{(2\pi\hbar)^3} f(\mathbf{r}, \mathbf{p}) = N, \tag{2.63}$$

where $\mathbf{p}$ is the atom momentum. The evolution of this distribution is described by the Boltzmann equation

$$\left(\frac{\partial}{\partial t} + \mathbf{v} \cdot \nabla + \mathbf{F} \cdot \frac{\partial}{\partial \mathbf{p}}\right) f = C(\mathbf{r}, \mathbf{p}), \tag{2.64}$$

where $\mathbf{v} = \mathbf{p}/M$, and $\mathbf{F} = -\nabla U(\mathbf{r})$ is the classical force. For s-wave collisions, which are those relevant for the trapped atoms, and are independent of energy, the collision integral can be written in the form

$$C(\mathbf{r}, \mathbf{p}) = \sigma \int \frac{d\Omega}{2\pi} \int \frac{d\mathbf{p}}{(2\pi\hbar)^3} (f_1 f_2 - f_1' f_2') \Delta v, \tag{2.65}$$

where $\Delta\mathbf{v} = (\mathbf{p}_1' - \mathbf{p}_2')/2M$ is the relative velocity of two atoms before collision, σ is the atom collision cross-section, Ω specifies the direction of scattering, and the usual notation for the Boltzmann collision integral is used [24]. This kinetic description can be simplified by assuming that in the evaporation process, the distribution function only depends on the particle energy, E. We can then use the energy distribution function $f(E)$, such that

$$f(\mathbf{r}, \mathbf{p}) = \int f(E) \delta(W(\mathbf{r}) - E) dE, \tag{2.66}$$

where $W(\mathbf{r}) = U(\mathbf{r}) + p^2/2M$. Multiplying the kinetic equation (2.64) by the delta function appearing in this relation, and integrating over $\mathbf{r}$ and $\mathbf{p}$, we are reduced to the equation

$$\rho(E) \frac{\partial f(E)}{\partial t} = C(E), \tag{2.67}$$

where we have defined

$$\rho(E) = \int d\mathbf{r} \int \frac{d\mathbf{p}}{(2\pi\hbar)^3} \delta(W(\mathbf{r}) - E). \tag{2.68}$$

This quantity can be interpreted as the energy density of the atomic states. The new Boltzmann collision integral is now

$$C(E) = \frac{M\sigma}{\pi^2\hbar^3}\int dE_1 \int dE_2 \int dE_1' \delta(E_1 + E_2 - E_1' - E)\rho(E_{\min}) \left[f(E_1)f(E_2) - f(E_1')f(E)\right], \tag{2.69}$$

where $E_{\min} = \min\left\{E_1, E_2, E_1'\right\}$. Assuming that the atoms with energy above a critical value U_0 evaporate, we have $f(E > U_0) = 0$. In that case, it can be shown that the kinetic equation (2.64) satisfies a truncated Boltzmann distribution of the form

$$f(E) = (n_0\lambda_T^3)e^{-E/T}H(U_0 - E), \tag{2.70}$$

where $H(x)$ is the Heaviside step-function. This solution can now be replaced in (2.66) yielding

$$f(\mathbf{r}, \mathbf{p}) = (n_0\lambda_T^3)e^{-W(\mathbf{r})/T}H[U_0 - W(\mathbf{r})]. \tag{2.71}$$

It is obvious that T cannot be, strictly speaking, the temperature of the system, because this is an open system which is not in thermal equilibrium, allowing for the energetic particles to scape. However, we can still call it a 'temperature' in the broad sense. Integration over momentum then leads to the density profile

$$n(\mathbf{r}) = n_0 e^{-W(\mathbf{r})/T}\left[\mathrm{Erf}\left(\sqrt{\zeta}\right) - 2\sqrt{\frac{\zeta}{\pi}}e^{-\zeta}\right], \tag{2.72}$$

where $\zeta = U_0 - U(\mathbf{r})/T$. Notice that this is different from the free density profile and, in particular, the number of atoms at the centre of the trap is smaller than in the absence of evaporation, $n(0) < n_0$.

Let us now consider the rate of change on the number of atoms remaining inside the trap. Using the truncated distribution (2.71) to integrate over the trapped energies $E < U_0$, we obtain from the kinetic equation (2.67)

$$\frac{dN}{dt} = -\int_{U_0}^{\infty}\rho(E)\frac{\partial f(E)}{\partial t}dE = -\frac{M\sigma}{\pi^2\hbar^3}\int dE_1 \int dE_2 \int dE_1'\, \rho(E_1')f(E_1)f(E_2), \tag{2.73}$$

where the energies E_1, E_2 and E_1' are upper bounded by U_0. Noting that in this range of integration the distribution functions are simple exponentials, we can easily get

$$\frac{dN}{dt} = -n_0^2\sigma\bar{v}e^{-\eta}V_{\mathrm{eff}}, \tag{2.74}$$

where $\bar{v} = \sqrt{8T/\pi M}$, and V_{eff} is an effective volume determined by

$$V_{\mathrm{eff}} = \frac{\lambda_T^3}{T}\int_0^{U_0}\left[(U_0 - E - T)e^{-E/T} + Te^{-\eta}\right]dE, \tag{2.75}$$

with $\eta = U_0/T$. This is a more refined version of Eq. (2.62). We can also compute the change of the mean kinetic energy per atom, reading

$$\frac{dW}{dt} = -\int_{U_0}^{\infty} dE\rho(E)E\frac{\partial f(E)}{\partial t}. \tag{2.76}$$

Using a similar procedure as in (2.73), we then get

$$\frac{dW}{dt} = \frac{dN}{dt}\left[U_0 + \left(1 - \frac{V'_{\text{eff}}}{V_{\text{eff}}}\right)T\right], \tag{2.77}$$

where a new effective volume appears, as

$$V'_{\text{eff}} = \frac{\lambda_T^3}{T}\int_0^{U_0}\left[Te^{-E/T} - (U_0 - E - T)e^{-\eta}\right] \tag{2.78}$$

Finally, the temperature evolution can be determined by using the equation of state, $W = CT + \mu N$, where $C = (\partial W/\partial T)_N$ is the heat capacity, and $\mu = (\partial W/\partial N)_T$ is the chemical potential. This then leads to

$$\frac{dT}{dt} = \frac{1}{C}\left[U_0 + \left(1 - \frac{V'_{\text{eff}}}{V_{\text{eff}}}\right)T - \mu\right]\frac{dN}{dt}. \tag{2.79}$$

This represents a refinement of the scaling law (2.60).

The above description can be reformulated using a quantum description. Quantum theories of evaporative cooling have been published over the years [25–29]. In this case, the Boltzmann distribution is replaced by a Bose distribution, and a similar procedure can lead to a truncated function of the form

$$f(\mathbf{r},\mathbf{p}) = \frac{H(A(\mathbf{r}) - E)}{Z^{-1}\exp(E/T) - 1}, \tag{2.80}$$

with

$$A(\mathbf{r}) = U_0 - U(\mathbf{r}) \quad \text{and} \quad Z(\mathbf{r}) = \exp\{[\mu - U(\mathbf{r})]/T\}, \tag{2.81}$$

where the effective potential can also be taken into account [29].

2.7 Sympathetic Cooling

The evaporative cooling technique can be applied to species that can be brought down to low enough temperatures (typically, at the micro-Kelvin region) with laser cooling. There are others, however, for which direct laser cooling is not possible or simply ineffective (as it is the case of molecules, whose electronic structure is too complicated). It is, however, possible to make use of inter-particle interactions to induce cooling to other particles which cannot be directly laser cooled. This is

the physical principle underlying the *sympathetic cooling* technique. For example, atomic ions that can be directly laser cooled are used to cool nearby ions or atoms, by way of their mutual Coulomb interaction. This includes most molecular ion species, especially large organic molecules [30]. The cooling of neutral atoms through sympathetic cooling was first demonstrated by Myatt et al. in 1997 [31]. Here, a technique with electric and magnetic fields was used, where atoms with spin in one direction were more weakly confined than those with spin in the opposite direction. The weakly confined atoms with a high kinetic energy were allowed to escape faster, lowering the total kinetic energy, resulting in a cooling of the strongly confined atoms.

A theoretical understanding of sympathetic cooling is quite simple to obtain after the discussion presented in the previous section. Let us consider a gas of N_2 particles with mass M_2 as the target specie, i.e., the one to be sympathetic cooled, and a 'buffer' gas (which can be laser cooled) of $N_1 = N_1(t)$ particles of mass M_1. The total kinetic energy in an harmonic trap ($\delta = 3/2$) is then given by $U_{\text{th}} = 3(N_1 + N_2)T$. Consider now that the buffer gas is set to evaporate with an energy cutoff $U_0 = \eta T$. The corresponding variation in the energy is given by

$$\frac{dU_{\text{th}}}{dN_1} = (\eta + \kappa)T, \tag{2.82}$$

where $0 \leq \kappa \leq 1$ is a parameter depending on the cutoff (the latter definition can be found in reference [23] and depends on the experimental details of the evaporation procedure). After rethermalization, the energy shift is determined by $E + dE = (N_1 + dN_1 + N_2)(T + dT)$. This corresponds to a temperature variation of the form

$$\frac{dT}{T} = \tilde{\alpha}\frac{dN_1}{N_1 + N_2}, \tag{2.83}$$

where $\tilde{\alpha} = (\kappa + \eta)/3 - 1$ is the new evaporation parameter. Assuming a constant cutoff η, we have

$$T = T_{\text{min}}\left(\frac{N_1 + N_2}{N_2}\right)^{\tilde{\alpha}}, \quad \text{with} \quad T_{\text{min}} = T(0)\left(\frac{N_2}{N_1(0)}\right)^{\tilde{\alpha}}. \tag{2.84}$$

As it immediately follows from Eq. (2.84), the minimum temperature T_{min} is reached when all the buffer atoms are evaporated ($N_1 = 0$). Because we are mainly interested in bringing the target specie down to quantum degeneracy, it is relevant to consider the phase space density $\varrho_j = 2.17 N_j \hbar\omega_j / T$ [32], where $j = 1, 2$ and ω_j are the trapping frequencies. Using the latter result, we can explicitly compute the phase-space of both the buffer and target gas

$$\varrho_j = 2.17 N_j \left(\frac{\hbar\omega_2}{T}\right)^3 \left[\frac{N_1(0)}{N_1 + N_2}\right]^{3\tilde{\alpha}}. \tag{2.85}$$

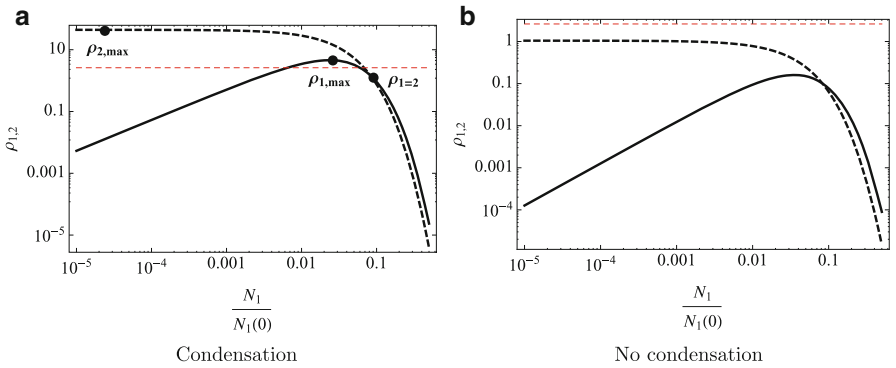

Fig. 2.5 Evolution of the phase-space density of both buffer (*dashed line*) and target (*full line*) atoms. The *red dashed line* corresponds to the phase-space density necessary to occur Bose-Einstein condensation ($\varrho_{\mathrm{BEC}} = 2.612$). (**a**) Condensation of both species. (**b**) No condensation. The parameters are discussed in the text and correspond to the experiment performed in Ref. [32]

After the evaporation of all the buffer atoms, we observe that the phase space density for the target atoms reaches its maximum value

$$\varrho_2^{\max} = \frac{2.17}{N_2^{(3\tilde{\alpha}-1)}} \left[N_1(0)^{\tilde{\alpha}} \frac{\hbar\omega_2}{T(0)} \right]^3, \tag{2.86}$$

where we have assumed that no evaporation of the target atoms occur and therefore N_2 is constant. Also, the buffer phase-space density increases first to a maximum value

$$\varrho_1^{\max} = \varrho_2^{\max} \left(\frac{\omega_1}{\omega_2} \right)^3 \frac{(3\tilde{\alpha}-1)^{(3\tilde{\alpha}-1)}}{3\tilde{\alpha}^{(3\tilde{\alpha})}} \tag{2.87}$$

and then decreases to zero. Another important value corresponds to the point where the phase-space density of the two species are equal

$$\varrho_{1=2} = \varrho_2^{\max} \left[1 + \left(\frac{\omega_1}{\omega_2} \right)^3 \right]^{-3\tilde{\alpha}}. \tag{2.88}$$

Notice that the relative positions between $\varrho_1^{\max}$, $\varrho_2^{\max}$ and $\varrho_{1=2}$ can be modified by changing the different evaporation parameters. In Fig. 2.5, the curves $\varrho_{1,2}$ in Eq. (2.85) are depicted for the evaporation of $N_1(0) = 10^8$ atoms to sympathetically cool down $N_2 = 6.5 \times 10^7$ target atoms. For definiteness, we use the experimental parameters of Ref. [32], with $\omega_2/\omega_1 = 2$, an initial temperature of $T(0) = 200\,\mu\mathrm{K}$ and $3\tilde{\alpha} - 1 > (\omega_1/\omega_2)^3$ to assure that both the species can be condensed (i.e., $\varrho_{1,2} > \varrho_{\mathrm{BEC}} = 2.612$). The physical meaning of this critical value will be explained in future chapters. If the mutual condensation condition $3\tilde{\alpha} - 1 > (\omega_1/\omega_2)^3$ is

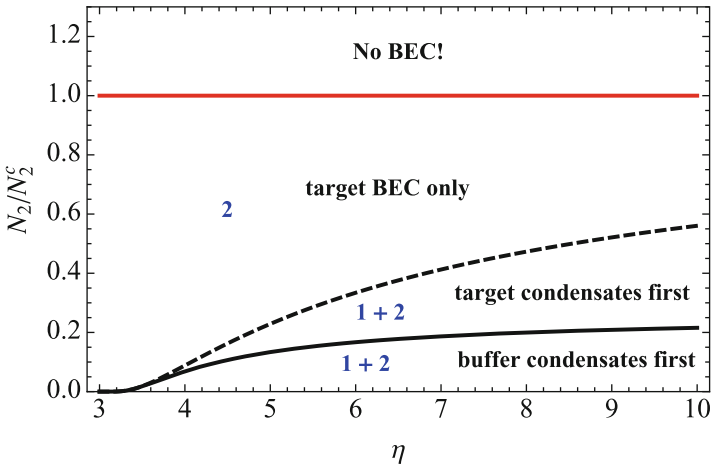

Fig. 2.6 Four different scenarios illustrating the features of sympathetic cooling, obtained for $\omega_2 = \sqrt{2}\omega_1$

satisfied, the buffer condenses first if $\varrho_{1,2} = 2.612$, otherwise the target condenses first. These previous conditions can be established as a function of the number of target atoms N_2. This allows us to define three critical numbers, N_2^a, N_2^b and N_2^c, for which $\varrho_{1=2}$, $\varrho_1^{\max}$ and $\varrho_2^{\max}$ simultaneously equal 2.612. In Fig. 2.6, we represent the critical curves N_2^a/N_2^c and N_2^b/N_2^c as a function of the cutoff η.

Another important property to be analyzed is the rate at which the cooling process occurs. So far, we have assumed that both the buffer and target atoms possess the same temperature (this is valid if the evaporation occurs slowly enough so the system can continuously thermalize). Let us now define the temperature average and difference between the two species, respectively given by $\Delta T = T_1 - T_2$ and $\bar{T} = (T_1 + T_2)/2$. Assuming that both specie obey a Maxwell-Boltzmann distribution, it is possible to compute the energy exchange $\Delta U_{\text{th}} = -2\Gamma\Delta T$, where Γ is the number of interspecies collisions per unit time, which can be approximately given by[2]

$$\Gamma \simeq \frac{N_1 N_2}{\pi^2 R_x R_y R_z}\sigma_{12}\bar{v}_{12}, \tag{2.89}$$

where $\bar{v}_{12} = \sqrt{k_B(T_1 + T_2)/\mathcal{M}}$ and $R_j = \sqrt{(k_B/\mathcal{M})(T_1/\omega_{1,j}^2 + T_2/\omega_{2,j}^2)}$, with $j = x, y, z$. Here, we have introduced the reduced mass

[2]For experimental reasons, Γ should be multiplied by a factor $e^{-\Delta^2/R_z^2}$, where $\Delta = g/\omega_{1,z}^2 - g/\omega_{2,z}^2$ represents the gravitational sag between the two clouds and $R_z = \sqrt{(k_B/\mathcal{M})(T_1/\omega_{1,z}^2 + T_2/\omega_{2,z}^2)}$ is the vertical size of the clouds. Near condensation, however, the effect of the sag is negligible and Eq. (2.89) holds. See Ref. [32] and references therein for further details.

$$\mathcal{M} = \frac{8(M_1 M_2)^2}{2(M_1 + M_2)^3}. \tag{2.90}$$

From this definition, we can easily write (for equal trapping frequencies, $\omega = \omega_1 = \omega_2$)

$$\frac{1}{\tau_{12}} = \frac{1}{\Delta T}\frac{d\Delta T}{dt} = \frac{N_1 + N_2}{3T}\frac{\omega^3 \sigma_{12}\mathcal{M}}{2\pi^2}. \tag{2.91}$$

It is possible to verify that this result is similar to that obtained in for a single specie, as discussed in the previous section. Noticing that we are here considering a trapped gas, Eq. (2.62) should be modified by replacing n_0 by $(N_1 + N_2)/\lambda_{\rm ho}$, which would simply yield [33] $\tau_{col}^{-1} = \gamma/3$, where $\gamma = N\omega^3 \sigma M/2\pi^2 T$ is the average collision rate in a harmonic trap. There are species for which the collision frequencies σ and σ_{12} interspecies are very similar, as it is the case of ^{87}Rb [34]. This implies that

$$\frac{1}{\tau_{12}} = \frac{1}{\tau_{\rm col,1}} + \frac{1}{\tau_{\rm col,2}}, \tag{2.92}$$

which remarkably states that thermalization between two different species is faster than thermalization of a single specie. And this is the key feature of sympathetic cooling: if the evaporation ramp is applied to cooling of the buffer alone, interspecies thermalization will remain efficient.

We stress that although we have considered the case of bosonic species for definiteness, this fact does not limit the present discussion and the same theory can be applied to the case of fermions. The only question that should be addressed in the latter is the absence of condensation.

References

1. M.O. Scully, S. Zubairy, *Quantum Optics* (Cambridge University Press, Cambridge/New York, 1997)
2. R. Loudon, *The Quantum Theory of Radiation* (Noth-Holland, Amsterdam, 1958)
3. C. Cohen-Tannoudji, J. Dupont-Roc, G. Grynberg, *Photons and Atoms: Introduction to Quantum Electrodynamics* (Wiley, New York, 1987)
4. S. Chu, L. Hollberg, J.E. Bjorkholm, A. Cable, A. Ashkin, Phys. Rev. Lett. **55**, 48 (1985)
5. S. Stenholm, The semiclassical theory of laser cooling. Rev. Mod. Phys. **58**, 699 (1986)
6. A.L. Migdall, J.V. Prodan, W.D. Philips, T.H. Bergeman, H.J. Metcalf, Phys. Rev. Lett., **54**, 2596 (1985)
7. J. Fortágh, C. Zimmermann, Magnetic microtraps for ultracold atoms. Rev. Mod. Phys. **79**, 235 (2007)
8. Yu.V. Gott, M.S. Yoffe, V.G. Tel'kovskii, Nucl. Fusion Suppl. Part 3, 1045 (1962)
9. D.E. Pritchard, Phys. Rev. Lett. **51**, 1336 (1983)
10. E.L. Raab, M. Printiss, A. Cable, S. Chu, D. Pritchard, Phys. Rev. Lett. **59**, 2631 (1987)
11. J. Dalibard, C. Cohen-Tannoudji, J. Opt. Soc. Am. B **6**, 2023 (1989)
12. C. Salomon, J. Dalibard, W. Phillips, A. Clairon, S. Guellati, Europhys. Lett. **12**, 683 (1990)

13. NIST Database, http://physics.nist.gov/PhysRefData/ASD/lines$_-$form.html (2009)
14. H.F. Hess, Phys. Rev. B **34**, 3476 (1986)
15. K.B. Davis, M.-O. Mewes, W. Ketterle, Appl. Phys. B **60**, 155 (1995)
16. W. Ketterle, N.J. van Druten, Adv. At. Mol. Opt. Phys. **37**, 181 (1996)
17. K.B. Davis et al., Phys. Rev. Lett. **75**, 3969 (1995)
18. J.M. Doyle, J.C. Sandberg, I.A. Yu, C.L. Cesar, D. Kleppner, T.J. Greytak, Phys. B **194**, 13 (1994)
19. K.M. O'Hara, M.E. Gehm, S.R. Granate, J.E. Thomas, Phys. Rev. A **64**, 051403(R) (2001)
20. P.J. Tol, W. Hogerworst, W. Vassen, Phys. Rev. A **70**, 013404 (2004)
21. D. Comparat, A. Fioretti, G. Stern, E. Dimova, B. Laburthe Tolra, P. Pillet, Phys. Rev. A **73**, 043410 (2006)
22. K. Berg-Sorensen, Phys. Rev. A **55**, 1281 (1997)
23. O.J. Luiten, M.W. Reynolds, J.T.M. Walraven, Phys. Rev. A **53**, 381 (1996)
24. R. Balescu, *Equilibrium and Non-equilibrium Statistical Mechanics* (Wiley, New York, 1975)
25. J. Tempere, F. Brosens, J.T. Devreese, Solid State Commun. **102**, 691 (1997)
26. M. Holland, J. Williams, J. Cooper, Phys. Rev. A **55**, 3670 (1997)
27. H. Wu, E. Arimondo, C.J. Cooper, Phys. Rev. A **55**, 3670 (1997)
28. D. Jaksch, C.W. Gardiner, P. Zoller, Phys. Rev. A **56**, 575 (1997)
29. M. Yamashita, M. Koashi, N. Imoto, Phys. Rev. A **59**, 2243 (1999)
30. S. Schiller, C. Lämmerzahl, Phys. Rev. A **68**, 053406 (2003)
31. C.J. Myatt, E.A. Burt, R.W. Ghrist, E.A. Cornell, C.E. Wieman, Phys. Rev. Lett. **78**, 586 (1997)
32. C. Delannoy, S.G. Murdoch, V. Boyer, V. Josse, P. Bouyer, A. Aspect, Phys. Rev. A **63**, 051602(R) (2001)
33. M. Arndt et al., Phys. Rev. Lett. **79**, 625 (1997); H. Wu, C.J. Foot, J. Phys. B **29**, L321 (1996); C.R. Monroe et al., Phys. Rev. Lett. **70**, 414 (1993); D.W. Snoke, J.P. Wolfe, Phys. Rev. B **39**, 4030 (1989)
34. P.S. Julienne et al., Phys. Rev. Lett. **78**, 1880 (1997)

http://www.springer.com/978-1-4614-5412-0

Physics of Ultra-Cold Matter
Atomic Clouds, Bose-Einstein Condensates and Rydberg Plasmas
Mendonça, J.T.; Terças, H.
2013, XXII, 398 p., Hardcover
ISBN: 978-1-4614-5412-0